An automatic building extraction method : Application to 3D-city modeling

Florent Lafarge, Pierre Trontin, Xavier Descombes, Josiane Zerubia, Marc Pierrot-Deseilligny

INRIA

INSTITUT NATIONAL DE RECHERCHE EN INFORMATIQUE ET EN AUTOMATIQUE

An automatic building extraction method : Application to 3D-city modeling

Florent Lafarge — Pierre Trontin — Xavier Descombes — Josiane Zerubia — Marc Pierrot-Deseilligny

N° 5925

May 2006

Thème COG

ISSN 0249-6399

An automatic building extraction method : Application to 3D-city modeling

Florent Lafarge * † , Pierre Trontin‡ , Xavier Descombes* , Josiane Zerubia * , Marc Pierrot-Deseilligny†

Thème COG — Systèmes cognitifs
Projets Ariana

Rapport de recherche n° 5925 — May 2006 — 29 pages

Abstract: In this report, we present an automatic building extraction method from Digital Elevation Models (DEMs). The DEMs are generated using an algorithm based on a maximum-flow formulation using three-view images. First, the building footprints are extracted from the DEMs through an automatic method based on marked point processes : they are represented by an association of rectangles. Then, these rectangular building footprints are regularized by improving both the connection of the neighboring rectangles and the facade discontinuity detection. We obtain structured footprints. These footprints are used for the 3D-city modeling by considering a parametric approach based on a skeleton process which allows to model the rooftops.

Key-words: satellite data, 3D-reconstruction, Digital Elevation Model, dense urban areas, building extraction, marked point processes

* Projet Ariana - INRIA/I3S - Sophia-Antipolis - email=Name.Lastname@inria.fr
† Institut Géographique National - Saint-Mandé - email=Name.Lastname@ign.fr
‡ Ecole Nationale Supérieure de l'Aéronautique et de l'Espace - Toulouse - email=Name.Lastname@supaero.org

Une méthode automatique d'extraction de bâtiments : Application à la reconstruction urbaine en 3D

Résumé : Dans ce rapport, nous présentons une méthode automatique d'extraction de bâtiments à partir de Modèles Numériques d'Elévation (MNE). Ces derniers sont générés par un algorithme fondé sur une formulation par flot maximal utilisant des images tri-stéréoscopiques. Dans un premier temps, les emprises de bâtiments sont extraites à partir de MNE par une méthode automatique fondée sur les processus ponctuels marqués : ces emprises sont réprésentées sous forme d'une association de rectangles. Ensuite, ces emprises rectangulaires sont régularisées en améliorant la connexion des rectangles voisins, et en détectant les discontinuitées de façades. Nous obtenons ainsi des emprises de bâtiments structurées. Ces emprises sont utilisées pour la reconstruction urbaine en 3D par une approche paramétrique fondée sur un processus de squelettisation des emprises permettant de modéliser les arêtes faîtières.

Mots-clés : données satellitaires, reconstruction 3D, Modèle Numérique d'Elévation, zones urbaines denses, extraction de bâtiments, processus de points marqués

Contents

1 Introduction

Faced with the growth of the urbanization, the automatic 3D-reconstruction of urban areas has become a topic of interest in the last few years. Various applications, such as the computing of electromagnetic wave propagation, the urban planning or the creation of virtual realities, require to be able to automatically build 3D-models with connected planar facets of towns.

Several automatic methods giving satisfactory results have been developed using aerial images or laser scanning. Aerial images are the most popular kind of data to deal with this type of problems. Different techniques have been proposed such as perceptual organization [11], polyhedral approach [1], parametric models [21] or structural approach [3]. Laser scanning is also very popular since the decrease of the acquisition cost. Although laser measurements are very accurate, laser scanning is known to have a low density of points. For instance, we can quote the parametric approach of [10].
Nowadays, this problem can be tackled by another type of data : the sub-metric satellite images. The future PLEIADES satellites are especially well adapted to deal with building 3D-reconstruction through the high resolution of images (0.7 meter) and the stereoscopic characteristics (three views - B/H=0.2). The main advantages of satellite data compared to aerial images are a high swath width and ground coverage. However, such data have a "relatively low" resolution and a "low" Signal to Noise Ratio (SNR) to deal with 3D-reconstruction problems. For example, PLEIADES simulations have 2 pixels per square meter density contrary to standard aerial images which have about 25 pixels per square meter. In this report, the method proposed will be applied to PLEIADES simulations on dense urban areas.

Automatic methods are mostly made up of two steps : the extraction of building footprints and the 3D-reconstruction. This first step is not necessary to some methods which directly use cadastral maps such as [2] or [6]. Many methods need building localization masks in order to initialize the footprint extraction algorithm, for example [3], [12], [20] or [21]. In this context, few city 3D-modelings are really fully-automatic, i.e. without building localization masks.

In this report, a fully-automatic footprint extraction method from Digital Elevation Models (DEMs) is presented. The DEMs are generated using an algorithm based on a maximum-flow formulation using three-view images.
First, the global shape of buildings are extracted by a method based on marked point processes : the building footprints are modeled by rectangle layouts. Then, these rectangular building footprints are regularized by improving the linking up of the neighboring rectangles

and detecting the facade discontinuities. The obtained building footprints are structured footprints : each element represents a specific part of an urban structure.
Results are applied to the 3D-city modeling by using a parametric approach. A skeleton process is used to model the rooftops of buildings. The different heights of buildings constitute parameters which are estimated and then regularized in order to favor the rooftop and getter of roof continuities.

2 DEM generation

The first step consists in generating DEMs from 3-view images. To do so, a method based on a multi-resolution implementation of a Cox and Roy optimal flow matching image algorithm [18] is used.

This method, detailed in [17], aims at solving the surface reconstruction problem formalized as a minimization of an energy. The last one is composed of a data attachment term and a regularizing term which depends on the smoothness of the surface. A multi-resolution approach is necessary to achieve reasonable processing times on extended areas and improve robustness by restraining matching ambiguities.
Figure 1 presents a result obtained from 3-view PLEIADES simulations on a single building (Amiens city hall - France).

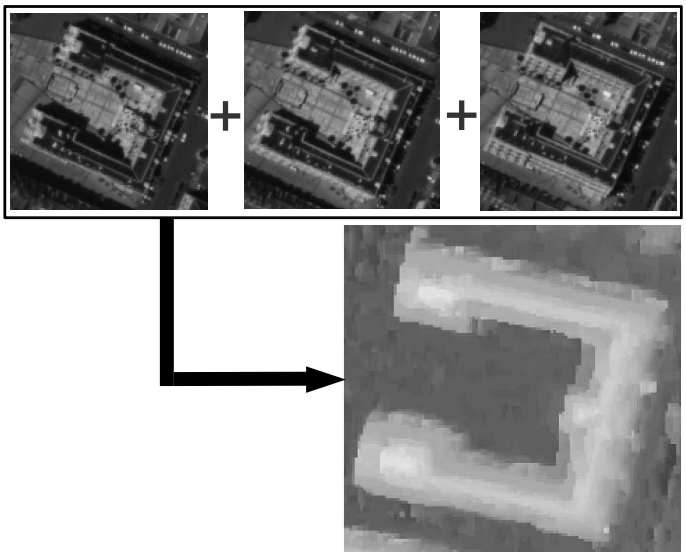

Figure 1: 3-view PLEIADES simulations of the Amiens city hall - France - (©CNES) and the associated DEM (©IGN)

3 Rectangular building footprints by marked point processes

High density of urban areas and complexity of human made objects make the building extraction difficult to achieve. We aim at developing an automatic method which doesn't need building localization maps or initialization states. To do so, a footprint extraction algorithm based on marked point processes is used [15].

3.1 Principle

This method is based on an object approach : it provides rectangle layouts which represent the building footprints. Faced with the complexity and the diversity of the building forms, such an approach is well adapted since it provides a modeling by simple geometric objects (i.e rectangles) and allows the introduction of a priori knowledge concerning the object layout and doesn't need initialization states. An energy is associated to each configuration. The global minimum of this energy is then found by applying a Reversible Jump Monte Carlo Markov Chain sampler embedded into a simulated annealing scheme [5].

3.1.1 Marked point process

Let consider a point process X living in $K = [0, X_{max}] \times [0, Y_{max}]$ which represents an image. X is a measurable mapping from a probability space $(\Omega, \mathcal{A}, \mathbb{P})$ to configurations of points of K :

$$\forall \omega \in \Omega, x_i \in K, X(\omega) = \{x_1, ..., x_n\} \tag{1}$$

A marked point process in $S = K \times M$ is a point process where each point is associated with a mark which allows to define an object. M is the mark space which allows, in our case, to describe random configuration rectangles :

$$M = [-\frac{\pi}{2}, \frac{\pi}{2}] \times [L_{min}, L_{max}] \times [l_{min}, l_{max}] \tag{2}$$

We note $\mathcal{C}$ the set of all finite configurations of objects of S. Figure 3 shows an element of S. Figure 2 represents a realization of a point process in K and a realization of a marked point process in S. More details on point processes and their applications can be found in [19].

3.1.2 Density formulation

We consider a marked point process X defined by an unnormalized density $h(.)$ from $\mathcal{C}$ to $\mathbb{R}$ and a reference intensity measure ν (defining a reference Poisson point process distribution).

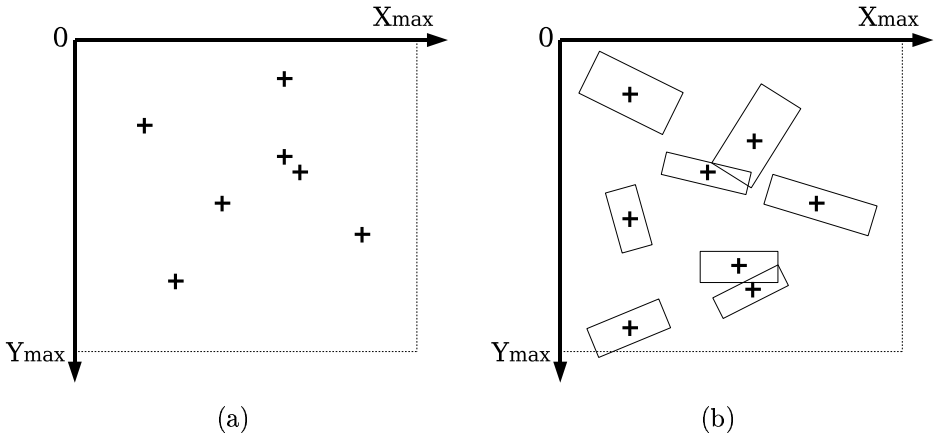

Figure 2: **(a) :** a realization of a point process in K **(b) :** a realization of a marked point process in S

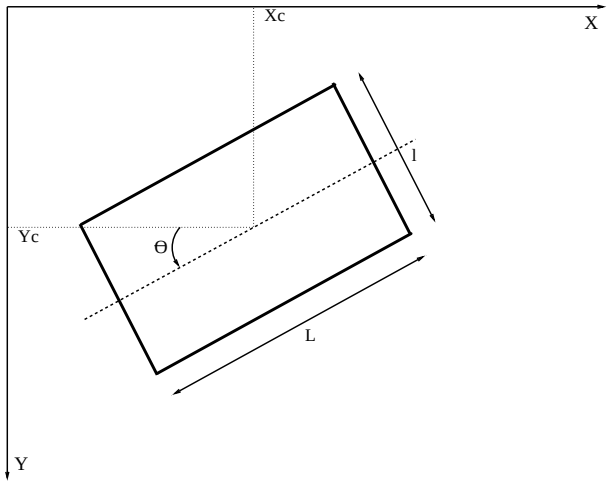

Figure 3: An element of S - $(X_c, Y_c) \in K$, the center of the rectangle - $(\theta, L, l) \in M$, the orientation of the rectangle, its length and its width

The unnormalized density $h(.)$ derives from three energies developed in the following and detailed in [14]. For a configuration $x \in \mathcal{C}$, it is given by :

$$h(x) = \exp - [U_{ext}(x) + U_{int}(x) + U_{excl}(x)] \tag{3}$$

External energy U_{ext} This term measures the quality of a configuration given the data, i.e. the DEM. It can be decomposed as a sum of energies $U_d(.)$ per object such as $U_{ext}(x) = \sum_{u \in x} U_d(u)$.
For each object $u \in x$, a local data energy $U_d(u)$ is computed by using a method which compares the DEM discontinuities to the borders of the object u.
Figure 4-(a) shows a part of a DEM , a rectangle (in white) and slices evenly disposed (in blue). We aim at extracting some points of interest from each slice and checking the coherence between these points and the rectangular shape of the object. Points of interest are detected using a profile simplification algorithm detailed in [14] - they represent DEM discontinuities on the slices (see figure 4-(b)). Then, three criteria of coherence are used to compute $U_d(u)$. The first criterion measures a volume rate (see figure 4-(c) - grey lines represent segments used to compute the volume rate). The second one corresponds to a moment rate (see figure 4-(d) - grey lines represent segments used to compute the moment rate). Eventually, the third criterion measures a localization rate (see figure 4-(e) - a gradient is boxed if it is close enough to the corresponding rectangle side).

Internal energy U_{int} The internal energy $U_{int}(x)$ allows to give a spatial structure to the configuration x. It can be seen as a regularizing term composed of three kinds of interaction between objects which favors alignment between rectangles, completion and some paving behavior. Figure 5 represents these three interactions.

Exclusion energy U_{excl} This term avoids redundant objects by penalizing the intersection of parallel rectangles. Such an exclusion energy is necessary since the redundant explanations of the data must be avoided and the attractive interactions must not be too strong.

3.1.3 Optimization

We want to find the configuration which maximizes the density $h(.)$. We search for the Maximum A Posteriori (MAP) estimator θ_{MAP}:

$$\theta_{MAP} = \arg\max_{\theta} h(\theta) \tag{4}$$

This is a non convex optimization problem in a high and variable dimension space $\mathcal{C}$. A Reversible Jump Monte Carlo Markov Chain sampler [4] [5] [19] embedded in a simulated annealing scheme is particularly well adapted to this problem.

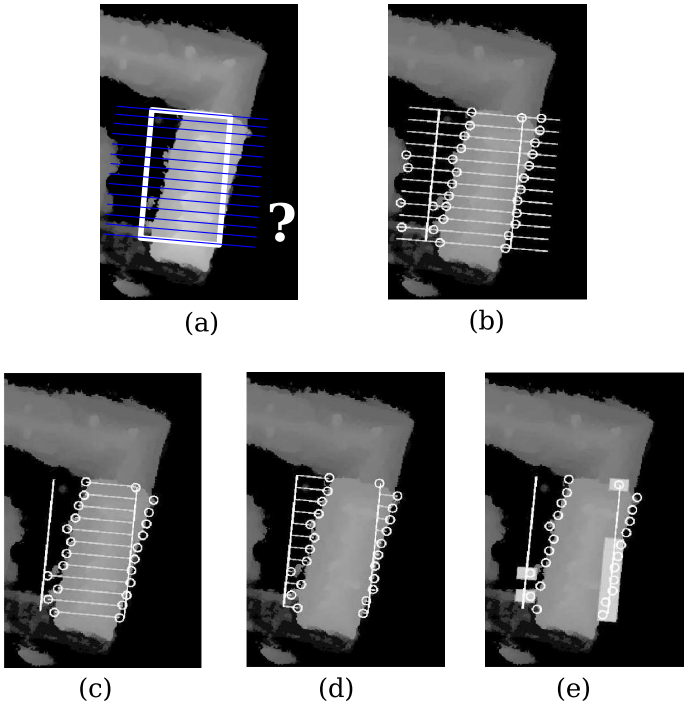

Figure 4: External energy - **(a) :** a part of a DEM , a proposed rectangle (in white) and slices (in blue) **(b) :** detected points of interest **(c) :** volume rate **(d) :** moment rate **(e) :** localization rate

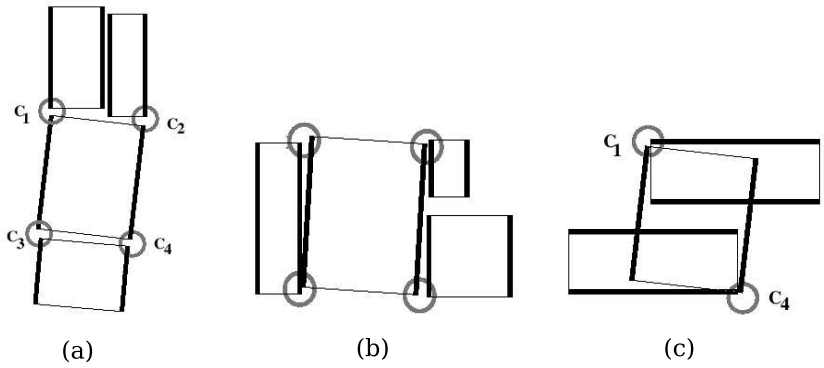

Figure 5: Internal energy - **(a) :** alignment interaction **(b) :** paving interaction **(c) :** completion interaction

It consists in simulating a discrete Markov Chain $(X_t)_{t\in\mathbb{N}}$ on $\mathcal{C}$ of invariant measure π (specified by the density $h(.)$) which performs small jumps between spaces of variable dimensions. One of the main advantages of such a sampler is that the chain asymptotically converges towards π for any initial configuration X_0. It means that initialization steps or building localization masks are not needed.

In practice, the RJMCMC sampler is embedded into a simulated annealing scheme : the density $h(.)^{\frac{1}{D_t}}$ is substituted to $h(.)$ where D_t is a sequence of temperatures which tends to zero as t tends to infinity. At the beginning of the algorithm (i.e. when the temperature is high), the process is not really selective : it allows to explore the density modes. When the temperature decreases, configurations which have a high density will be favored. However, it is necessary to impose conditions concerning the temperature decay to ensure the algorithm convergence. A logarithmic decrease $D_t = \frac{c}{log(1+t)}$, where c is a constant high enough to allow the exploration of local minima of energy, permits to be sure that the algorithm converges.

3.2 Results

This building extraction method gives satisfactory results for a large range of DEMs (see [13] for results on optical and LASER DEMs). In the following, we only present results on optical satellite DEMs.

3.2.1 Results on PLEIADES simulations

Figure 7 presents results from PLEIADES simulations on Amiens city (France). Figure 6 shows two results on dense urban areas. Results are satisfactory : a large majority of urban structures are correctly detected.

However, we can see two drawbacks. First, some building footprints have not been detected. They correspond to low flat buildings of inner courtyards that the proposed method cannot detect since these buildings have low DEM discontinuities. Second, the building extraction method detects some trees (figure 6-(c)). However, this default can be corrected by introducing a vegetation mask in the process.

3.2.2 Comments

The results are satisfactory in a satellite and automatic context. However, applying directly a 3D-reconstruction process from these rectangular building footprints engenders artefacts in the 3D-results as it is shown in [9]. These artefacts are mainly due to non optimal connections between neighboring rectangles (see Figure 8). That is why these rectangle layouts need to be regularized, especially the linking up between neighboring rectangles. We address this problem in the following section.

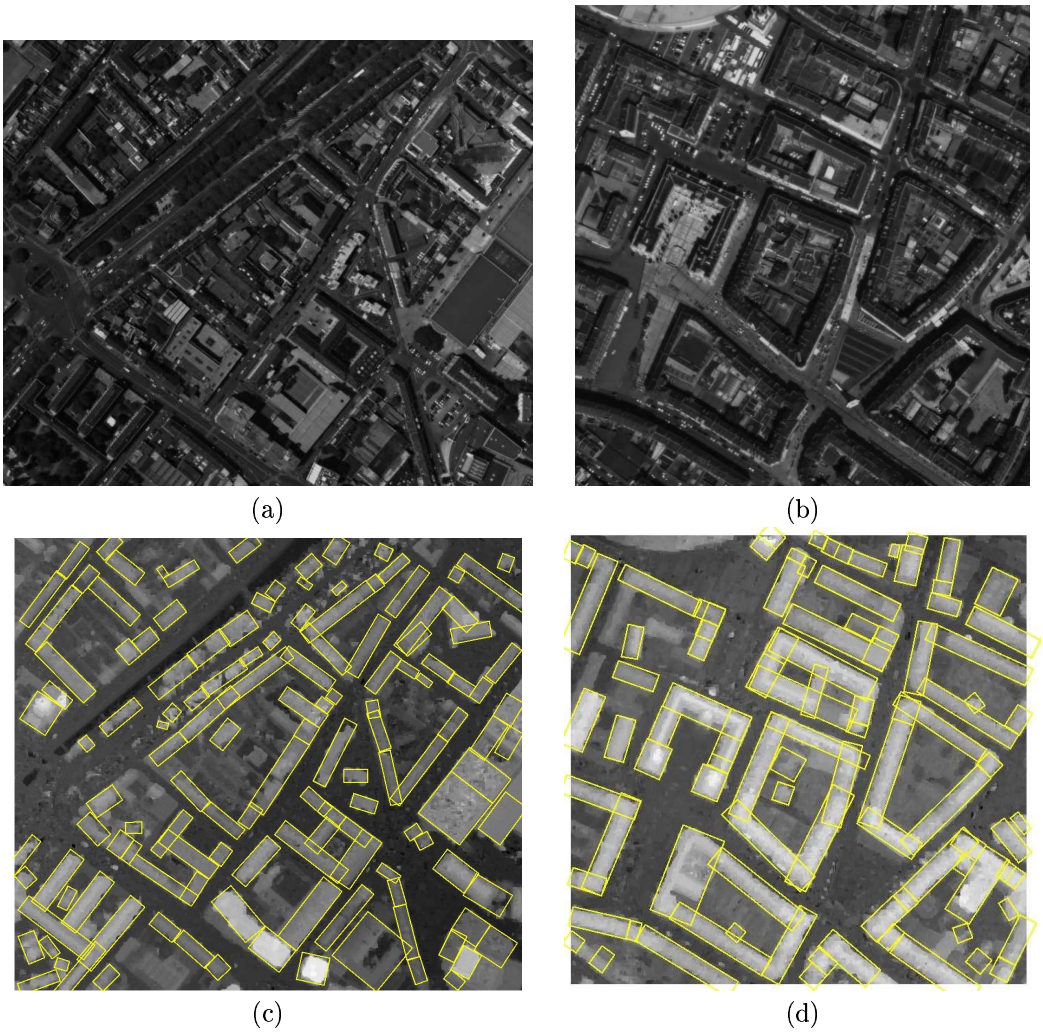

Figure 6: **(a)&(b) :** PLEIADES simulations on Amiens areas (©CNES) **(c)&(d) :** associated DEMs and results of rectangular building extractions (©INRIA)

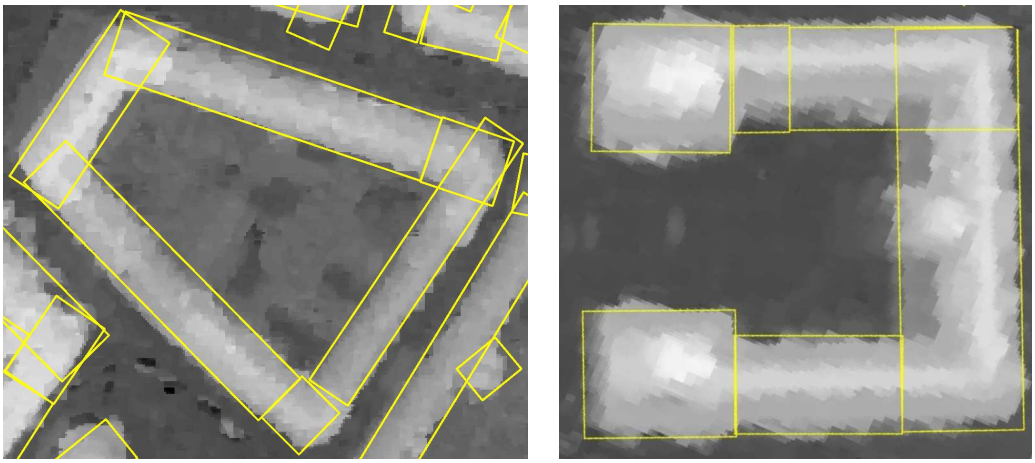

Figure 7: Examples of building extraction results (©INRIA)

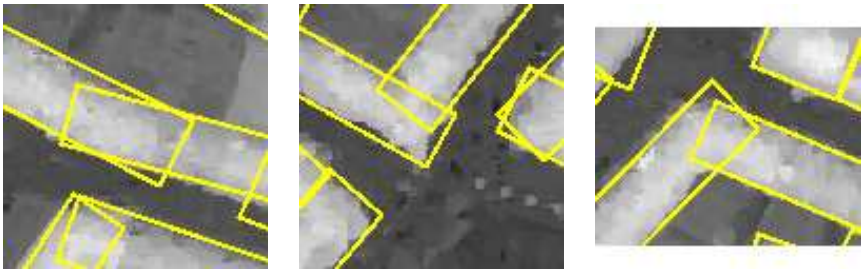

Figure 8: Examples of non optimal connections between neighboring rectangles (©INRIA)

4 Regularization : towards structured footprints

The rectangle layouts are regularized by improving, firstly, the connection between neighboring rectangles (through a local fusion of rectangles) and, secondly, the position of facades (through a facade discontinuity detection). At the end, we obtain structured building footprints whose elements are correctly connected : each one represents a specific part of an urban structure.

4.1 Connection between neighboring rectangles

We aim at improving the connection between neighboring rectangles. Figure 9-(a) represents a typical configuration of two neighboring rectangles that we want to connect.

Generalizing 3D volumes, such as in [7], could allow to improve the linking up between neighboring rectangles, nevertheless some building details would be lost. Applying small perturbations on the rectangle parameters could improve the connection. However, such a method cannot be used since the information related to the general layout of rectangles will be lost. The chosen solution consists in merging the neighboring rectangles, i.e. morphing two rectangles into polygons which are perfectly connected as we can see on figure 9-(b).

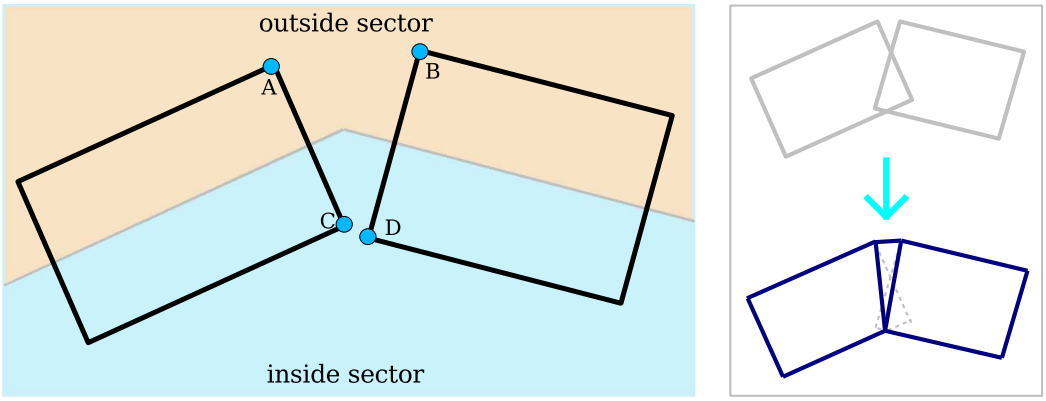

(a) (b)

Figure 9: **(a) :** two neighboring rectangles **(b) :** example of a fusion

4.1.1 Fusion configurations

We aim at merging two neighboring rectangles (R_1, R_2), it means we search for connecting both point A and point B (outside sector), and point C and point D (inside sector) of fig-

ure 9-(a) in order to create polygons $(P_i)_{i\in\mathbb{N}^*}$ which are perfectly connected (see figure 9-(b)).

It exists many relative positions of two neighboring rectangles which depend on the width of the rectangles, their orientation and their distance. Faced with the high number of possibilities, an exhaustive description of all the fusion configurations will be very heavy. We have chosen to restrict the number of possibilities to 16 fusion configurations.

Figure 10 presents 4 connection configurations of the outside sector (it means the connection between point A and point B). These configurations are based on intersections of straight lines defined by the width and length of rectangles. Concerning the inside sector (i.e the connection between point C and point D), the 4 same configurations are allowed (see figure 11). Eventually, 16 fusion configurations are proposed. They allow to describe a large range of the most realistic cases. Figure 12 shows a fusion configuration in three different rectangle relative positions.

4.1.2 Cost function

In order to select the most adapted fusion configuration, we define a cost function which measures the coherence between the proposed configuration and the data represented by both the DEM and the two initial rectangles. This cost is composed of three terms :

$$C = C_{DEM} + \omega_1 C_{recovering} + \omega_2 C_{contour} \tag{5}$$

where ω_1 and ω_2 represent weights which are tuned by trial and error.

DEM cost The DEM term allows to define the quality of the proposed configuration, given the DEM. To do so, we estimate the rate of high intensity pixels which are inside the proposed footprint (i.e. pixels which correspond to pieces of building). The higher the rate, the lower the cost. The high intensity pixels are detected by thresholding : the threshold value corresponds to half a floor height with respect to the ground altitude. Let consider N, the number of these high intensity pixels inside the proposed footprint, and N_t, the volume of the footprint (i.e. the total number of pixels). Then, the DEM cost can be written as follows :

$$C_{DEM} = 1 - \frac{N}{N_t} \tag{6}$$

Recovering cost This term provides a surface criterion : it corresponds to the recovering rate between the proposed configuration and the two rectangles. Let consider R_1 and R_2, the two initial rectangles, and P, the union of polygons defined by the proposed fusion. Then, the recovering term is given by :

$$C_{recovering} = \frac{\mid Surface(P) - Surface(R1 \cup R2) \mid}{Surface(R1 \cup R2)} \tag{7}$$

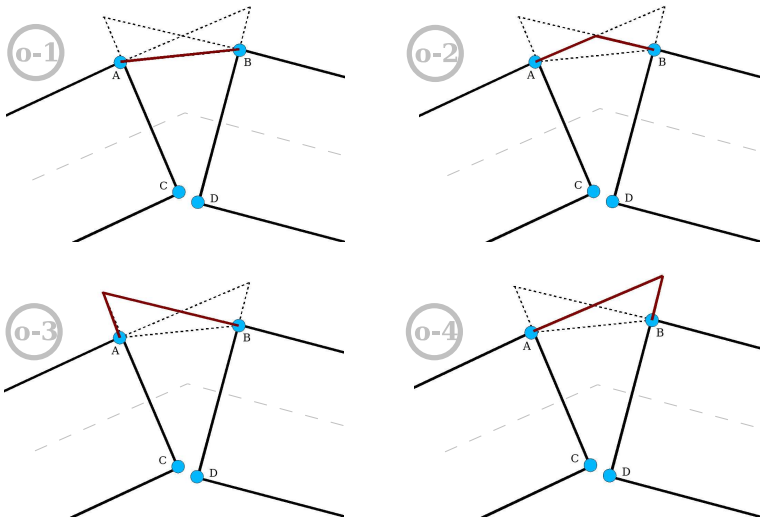

Figure 10: The 4 connection configurations of the **outside** sector

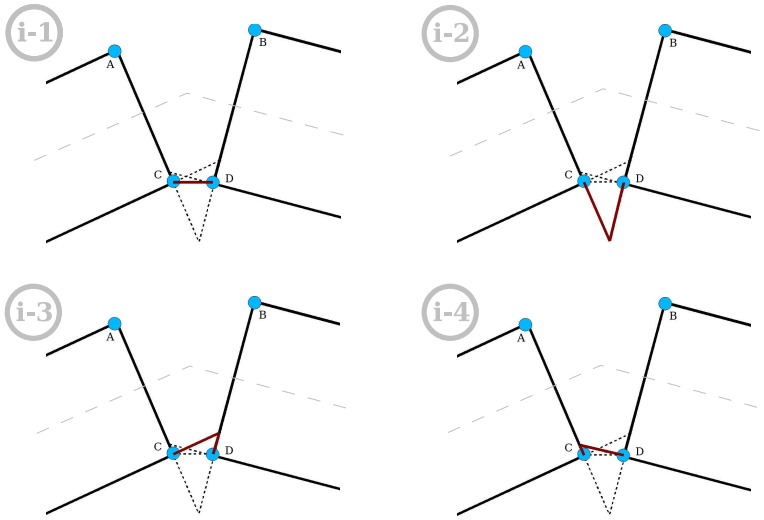

Figure 11: The 4 connection configurations of the **inside** sector

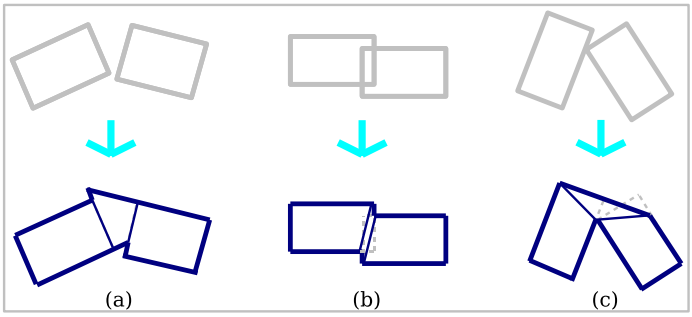

Figure 12: A fusion configuration (o-3 / i-3) in three different rectangle relative positions

For example, the configuration of figure 12-(b) is favored (the recovering cost is null) contrary to the one of figure 12-(a).

Contour cost This term allows to estimate the contour coherence between the proposed configuration and the two initial rectangles. This cost penalizes complex fusions as we can see on figure 13. Let consider L_{in} (respectively L_{out}), the total length of the inside sector polygons P (respectively outside sector) and L_1 and L_2, the length of the two rectangles. The contour cost is defined as follows :

$$C_{contour} = \frac{L_{out} + L_{in}}{2 \times (L_1 + L_2)} \tag{8}$$

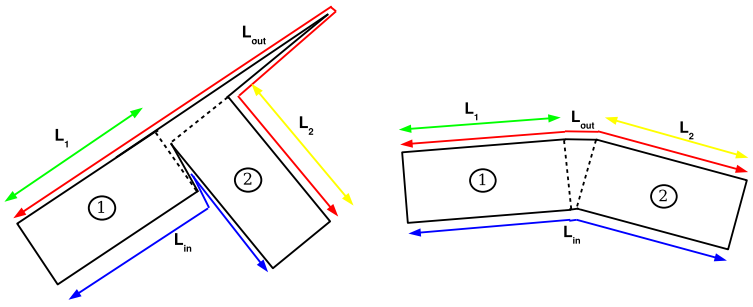

Figure 13: Contour cost **left :** configuration penalized by the contour cost **right :** favored configuration

4.1.3 algorithm

Rectangular footprints are morphed into polygonal footprints whose elements are perfectly connected. To do so, the fusion process between two rectangles is applied for each couple of neighboring rectangles which are positioned in series (a rectangle is positioned in series if it owns at most two neighbors at two facing sides). These fusions "in series" are well adapted to these rectangle layouts since a large majority of rectangles is positioned in series. It is due to the internal field of the rectangular footprint extraction method (see section 3.1.2) which allows to regularize the rectangles, and especially favors their alignments.

The algorithm consists in merging all the neighboring rectangles which are positioned "in series". If several neighboring rectangles are positioned "in parallel", the couple of rectangles which proposes the longest train of fusions is merged.
Consequently, instead of considering parts of buildings represented by rectangles, we work on complete buildings. Each building b is associated with a set of connected polygons $\mathcal{P}_b$.

Figure 14 presents the result from the rectangular footprints of the figure 7. This result is satisfactory : the artefacts of rectangle connections have disappeared.

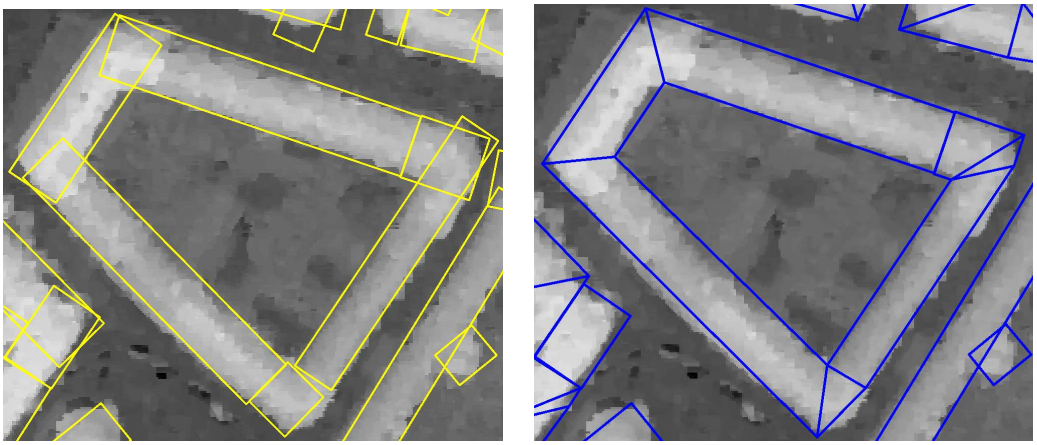

(a) (b)

Figure 14: **(a) :** rectangular footprints (©INRIA) **(b) :** footprints with fusion of rectangles (©INRIA/CNES/IGN)

4.2 Facade discontinuity detection

The second improvement consists in detecting the facade discontinuities in the building footprints. In fact, several roof heights can exist inside a footprint as we can see in figure 15-(a).

To do so, a rooftop profile is computed for each footprint (see figure 15-(b)). This profile is obtained by estimating the average roof height (i.e. Z) in a sliding window. Then, the high gradients are detected by applying a thresholding on the profile derivative (see figure 15-(c)). The threshold is a parameter which has been set up to 2 (this value corresponds to the Z-variation to X-variation ratio). Finally, the selected gradients are accumulated (figure 15-(d)) in order to obtain the facade discontinuities presented on figure 15-(e).
Figure 16 shows the result from the footprints of the figure 7. This result represents "structured building footprints" since each element represents a specific part of an urban structure.

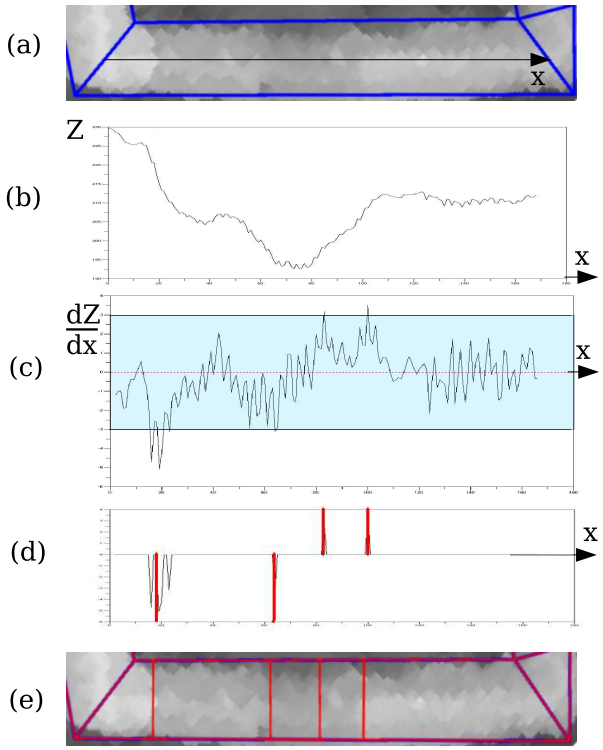

Figure 15: Facade discontinuity detection **(a)**: initial footprint **(b)**: rooftop profile **(c)**: gradient selection **(d)**: gradient accumulation **(e)**: resulted footprint with facade discontinuities (in red)

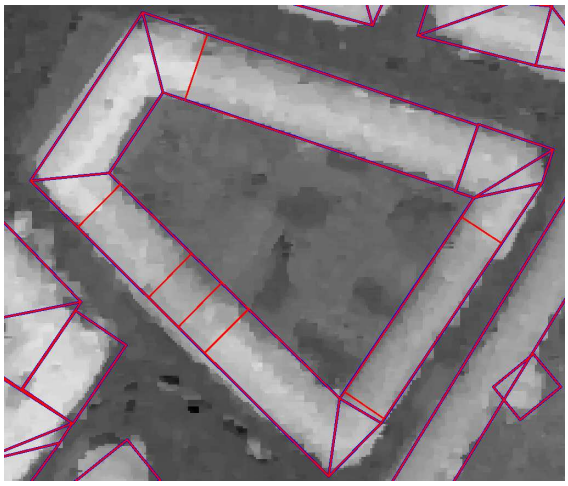

Figure 16: Building footprints with facade discontinuities (©INRIA/CNES/IGN)

4.3 Results

Figures 17 and 18 show results of structured building footprints (c) associated with PLEIADES simulations (a) and the rectangular footprints (b).
These results are satisfactory since the footprints are now regularized : rectangle connections have been improved and facade discontinuities have successfully been detected. However, results always present defaults concerning footprint under-detection which has been underlined in section 3.2.

5 Application to 3D-city modeling

This section presents an application of the previous results : the 3D-city modeling. The structured building footprints provide useful knowledge concerning the localization of buildings, the change of rooftop direction and the facade discontinuities. It means that these footprints give 3D information. We propose a building 3D-reconstruction process using these structured footprints. It is based on a parametric approach which has been chosen since it is particularly robust. However, this approach proposes restricted 3D-models.

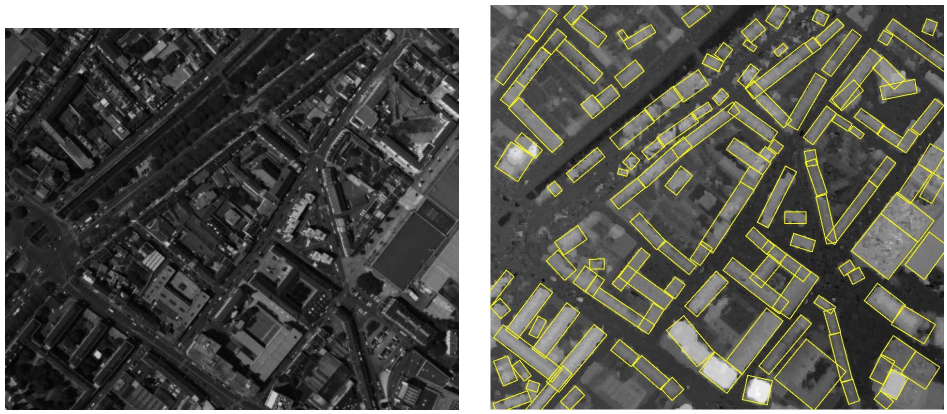

(a) (b)

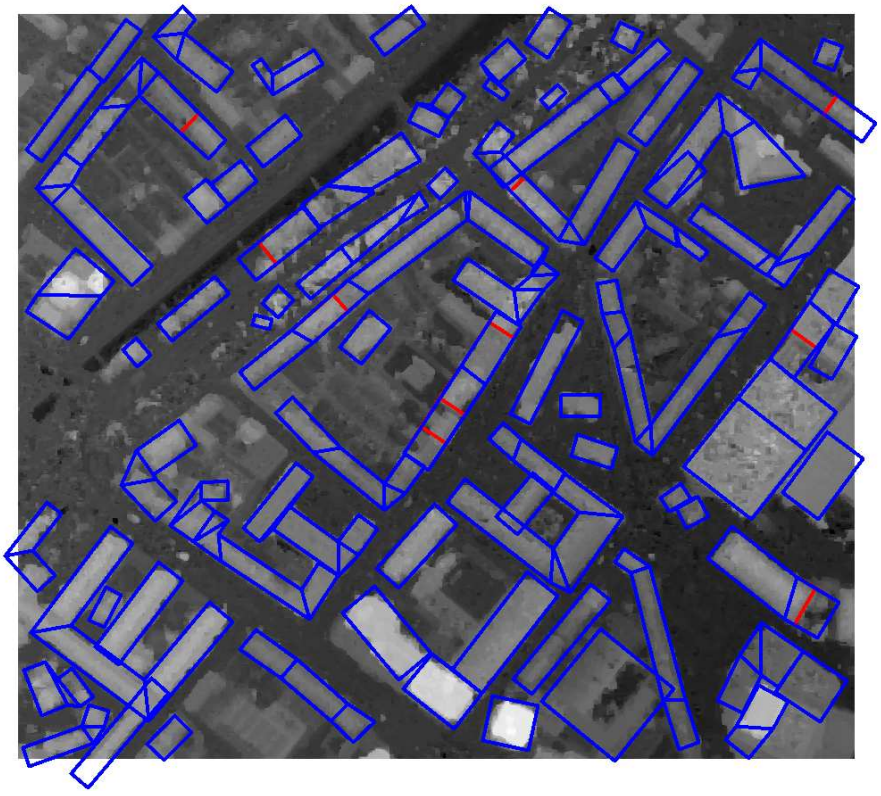

(c)

Figure 17: **(a) :** PLEIADES simulation on a piece of Amiens (©CNES) **(b) :** rectangular building footprints (©INRIA) **(c) :** structured building footprints (©INRIA/CNES/IGN)

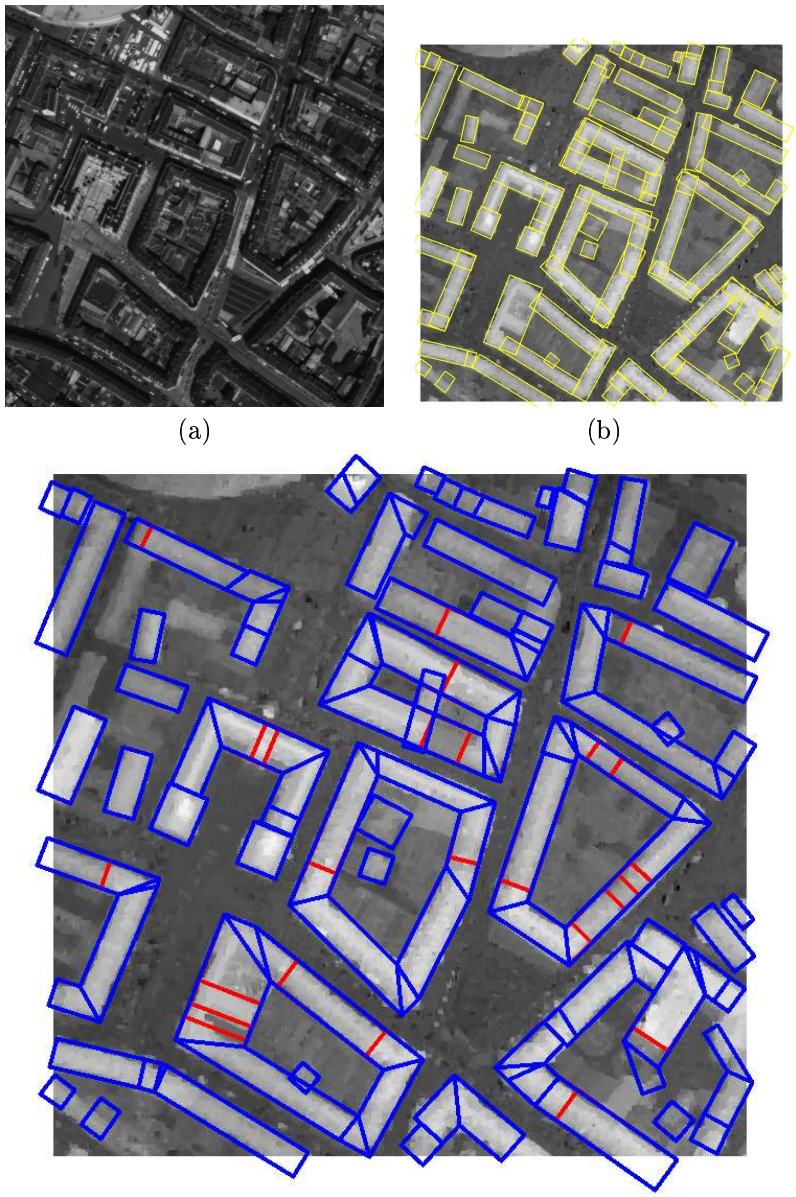

Figure 18: **(a) :** PLEIADES simulation on Amiens downtown (©CNES) **(b) :** rectangular building footprints (©INRIA) **(c) :** structured building footprints (©INRIA/CNES/IGN)

5.1 Skeleton process of the footprints

The proposed parametric method is based on a skeleton process of the structured footprints which allow to model the rooftops of buildings. It is a very simple process : roofs are constrained to be symmetric two-planes. Such a process has been used in [2]. In other words, for each building b, we consider the median axis of the connected polygon set $\mathcal{P}_b$ as the rooftops. The roof forms are fully determined by the structured building footprints : it allows to reduce the computing time comparatively to other approaches.
Figure 19 represents the result of the skeleton process.

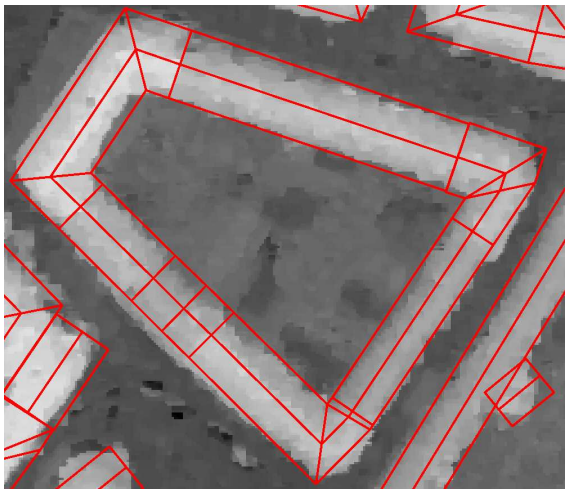

Figure 19: projected roof form using a skeleton process (©INRIA/CNES/IGN)

5.2 Setting of the building heights

The different heights of buildings constitute the parameters of the model. For each polygon of $\mathcal{P}_b$, a getter of roof height and a rooftop height are estimated by a method developed in a previous work [8]. These heights are then regularized on all the building b by using the "K-means" algorithm including a regularizing term. A similar algorithm using an entropic term has been proposed in [16]. The advantage of such an algorithm is that the number of classes does not need to be known a priori. It allows to favor the rooftop continuity and reduces the presence of artefacts.

Let us consider a set of N connected polygons $\mathcal{P}_b$ representing the footprint of a building b (see, for example, figure 16) and Hg_i, the estimated height of the getter of roof of the i^{th} polygons ($i \in [1, N]$). The proposed "K-means" algorithm including a regularizing term

consists in searching for c_j, the centroid of the j^{th} class, which minimizes the criterion J defined as follows :

$$J = \sum_{j=1}^{C} \sum_{i=1}^{N} d^2(Hg_i, c_j) - \alpha C \tag{9}$$

where C represents the number of classes (which is unknown).

The criterion J is composed of two terms. The first one corresponds to the classical criterion of the "K-means" algorithm. The second one, which is weighted by the parameter α, represents a priori knowledge on the classes. This term linearly favors a low number of classes. Each height Hg_i is associated with its centroid c_j which represents the final regularized height of the getter of roof. The same process is applied for the rooftop heights.

Figure 20 represents examples of a reconstructed building. The first one (a) is obtained without regularizing building heights : we can see the presence of artefacts through the bad adjustments of the rooftop heights and getter of roof heights. The second building (b) is regularized.

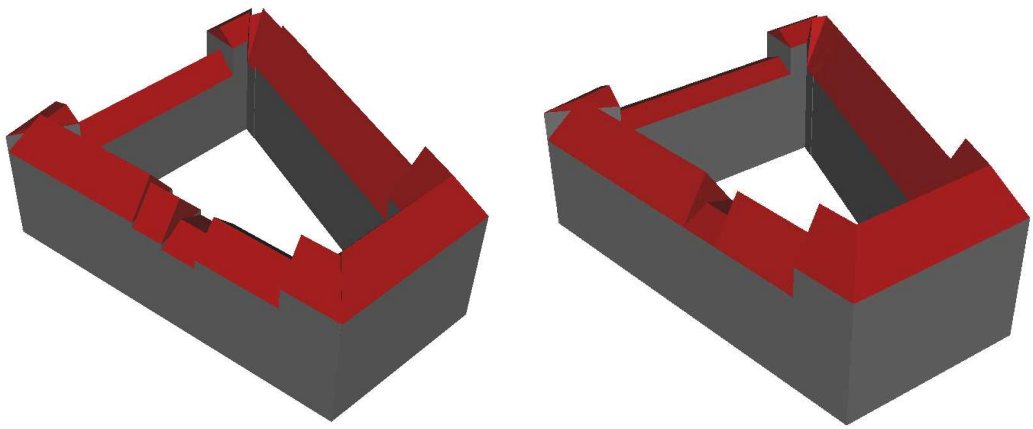

(a) (b)

Figure 20: **(a)** : non-regularizing 3D-reconstruction **(b)** : regularizing 3D-reconstruction (©INRIA/CNES/IGN)

5.3 Results

Results have been obtained on Amiens city (France). The associated 3D-ground truths have been semi-automatically established by the French Geographic Institute (IGN) from aerial images (0.2 meter resolution) and ground maps.

Figure 21 presents an example of building 3D-reconstruction (a) associated with the structured building footprints (b) and the 3D-ground truth (c). This result is satisfactory compared to the 3D-ground truth. The proposed modeling does not allow to represent some details. However, the global shape is respected and the generalization level is acceptable for satellite data in an automatic context.

Figures 22 and 23 show results on two Amiens areas. Figures 22/23-(b) represent structured building footprints associated with the DEM of the areas. The 3D-results (figures 22/23-(a)) are satisfactory compared to the associated 3D-ground truths (figures 22/23-(c)). Even if the 3D-modeling is simple (the roof forms are constrained to be symmetric two-planes), a majority of urban structures is close to reality. Moreover, these results are aesthetically satisfactory compared, for example, to results presented in [8].

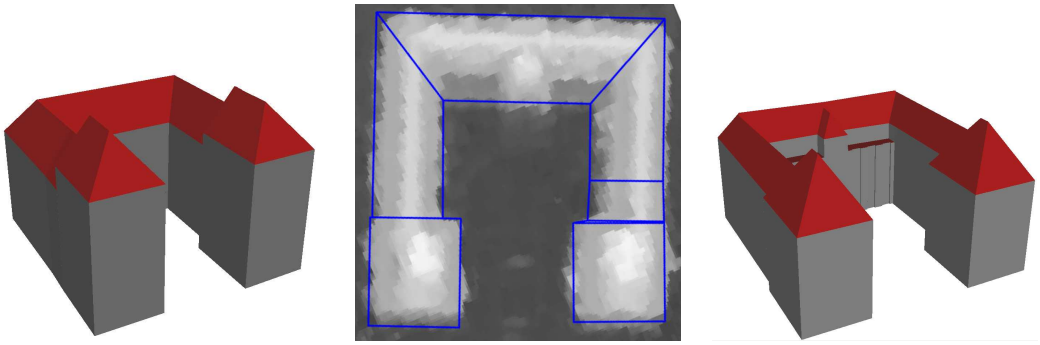

(a) (b) (c)

Figure 21: **(a) :** 3D-result of Amiens city hall (©INRIA/CNES/IGN) **(b) :** structured building footprints **(c) :** 3D-ground truth (©IGN)

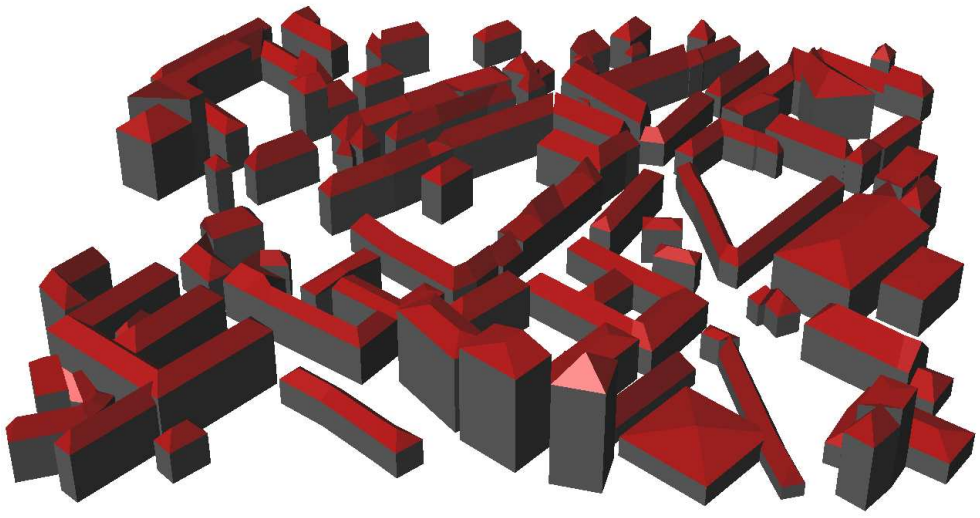

(a)

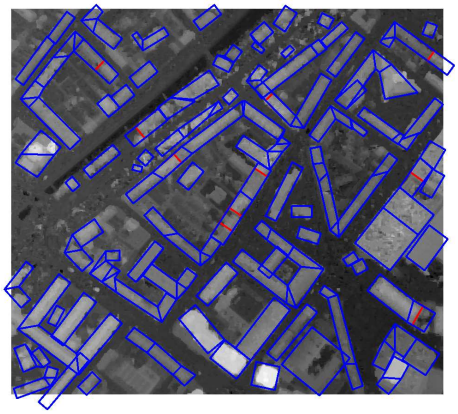

(b)

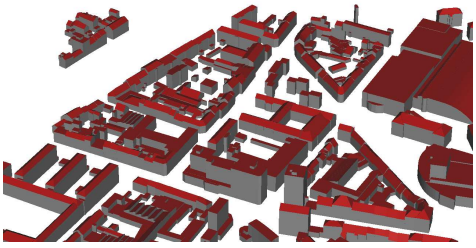

(c)

Figure 22: **(a) :** 3D-result (©INRIA/CNES/IGN) **(b) :** structured building footprints **(c) :** 3D-ground truth(©IGN)

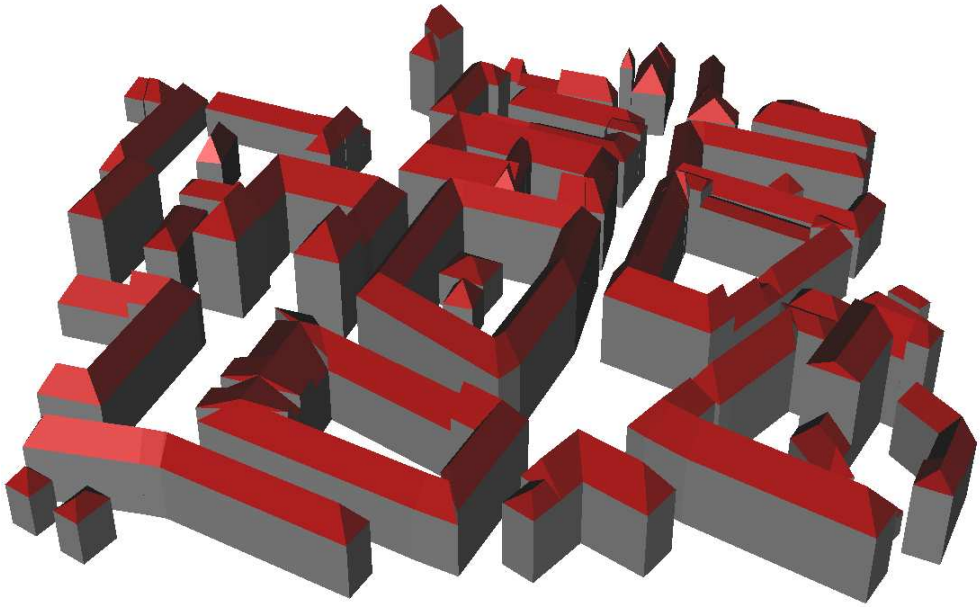

(a)

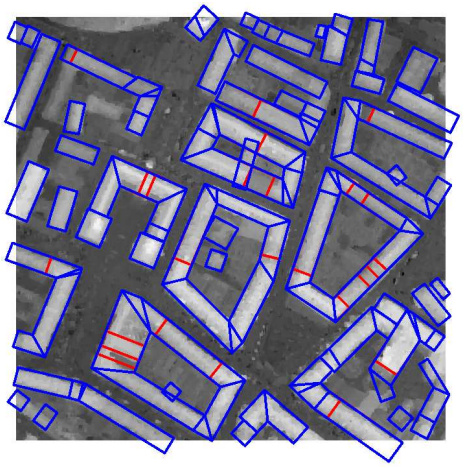

(b)

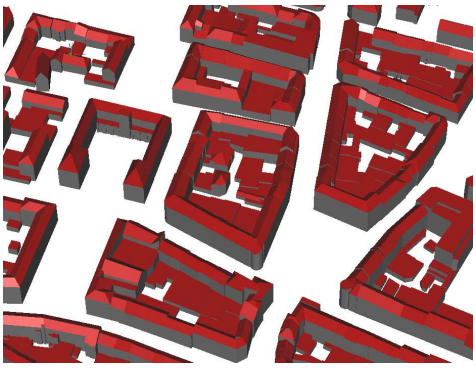

(c)

Figure 23: **(a) :** 3D-result (©INRIA/CNES/IGN) **(b) :** structured building footprints **(c) :** 3D-ground truth(©IGN)

6 Conclusion

A method for the building footprint extraction has been proposed in this report. This method is fully-automatic : building localization maps or initialization states are not needed. It provides structured footprints where each element represents a specific part of a building and is perfectly connected to the neighboring ones. The obtained results are satisfactory and the method seems to be efficient even on dense urban areas using HR satellite data.

An extension to the 3D building reconstruction has been proposed : it allows to give satisfactory 3D city modelings. Even if this method is very simple (the roof forms are constrained to be symmetric two-planes), a majority of urban structures is close to reality and results are aesthetically correct thank to the lack of artefacts in the structured building footprints.

In the future, we should extend the roof form possibilities in order to have more realistic models. To do so, we could use a grammar of 3D-models which include more complex roof forms such as dissymmetric two-planes or gambrel roofs.

Acknowledgments

The first author would like to thank the French Geographic Institute (IGN) and the French Space Agency (CNES) for partial financial support during his PhD. The authors thank the French Space Agency (CNES) for providing PLEIADES simulations.

References

[1] C. Baillard and A. Zisserman. A plane-sweep strategy for the 3D reconstruction of buildings from multiple images. In *19th ISPRS Congress and Exhibition*, Amsterdam, Netherlands, 2000.

[2] D. Flamanc and G. Maillet. Evaluation of 3D city model production from PLEIADES HR satellite images and 2D ground maps. In *URBAN*, Tempe, U.S., 2005.

[3] F. Fuchs and H. Le Men. Efficient subgraph isomorphism with a-priori knowledge. Application to building reconstruction for cartography. *Lecture Notes in Computer Science*, (1876), Springer, 2000.

[4] C.J. Geyer and J. Moller. Simulation and likehood inference for spatial point processes. *Scandinavian Journal of Statistics*, Series B(21):359–373, 1994.

[5] P.J. Green. Reversible Jump Markov Chains Monte Carlo computation and Bayesian model determination. *Biometrika*, 57:97–109, 1995.

[6] H. Jibrini, M. Pierrot-Deseilligny, N. Paparoditis, and H. Maître. Automatic building reconstruction from very high resolution aerial stereopairs using cadastral ground plans. In *19th ISPRS Congress and Exhibition*, Amsterdam, Netherlands, 2000.

[7] M. Kada. 3D building generalization based on half-space modeling. In *workshop ISPRS, commission II*, Hannover, Germany, 2006.

[8] F. Lafarge, X. Descombes, J. Zerubia, and M.P. Deseilligny. A parametric model for automatic 3D building reconstruction from high resolution satellite images. Research Report 5687, INRIA, september 2005.

[9] F. Lafarge, X. Descombes, J. Zerubia, and M.P. Deseilligny. An automatic 3D city model : a Bayesian approach using satellite images. In *Proc. IEEE International Conference on Acoustics, Speech and Signal Processing (ICASSP)*, Toulouse, France, May 2006.

[10] H. Maas. Fast determination of parametric house models from dense airborne laser-scanner data. In *ISPRS workshop on Mobile Mapping Technology*, 1999.

[11] R. Nevatia and K. Price. Automatic and interactive modeling of buildings in urban environments from aerial images. In *Proc. IEEE International Conference on image Processing (ICIP)*, New York, 2002.

[12] H. Oriot. Statistical snakes for building extraction from stereoscopic aerial images. In *ISPRS Conference on Photographic Image Analyses*, Hannover, Germany, 2003.

[13] M. Ortner. *Processus ponctuels marqués pour l'extraction automatique de caricatures de bâtiments à partir de modèles numériques d'élévation.* PhD thesis, University of Nice-Sophia Antipolis, 2004.

[14] M. Ortner, X. Descombes, and J. Zerubia. Automatic 3D land register extraction from altimetric data in dense urban areas. Research Report 4919, INRIA, France, September 2003.

[15] M. Ortner, X. Descombes, and J. Zerubia. Building extraction from Digital Elevation Model. In *Proc. IEEE International Conference on Acoustics, Speech and Signal Processing (ICASSP)*, Hong Kong, 2003.

[16] G. Palubinskas, X. Descombes, and F. Kruggel. An unsupervised clustering method using the entropy minimization. In *Proc. International Conference on Pattern Recognition (ICPR)*, Brisbane, Australia, August 1998.

[17] M. Pierrot-Deseilligny and N. Paparoditis. A multiresolution and optimization-based image matching approach : an application to surface reconstruction from SPOT5-HRS stereo imagery. In *Workshop ISPRS commission I*, Ankara, Turkey, 2006.

[18] S. Roy and I.J. Cox. A maximum-flow formulation of the n-camera stereo correspondence problem. In *Proc. International Conference on Computer Vision (ICCV)*, Bombay, 1998.

[19] M.N.M Van Lieshout. Markov point processes and their applications. In *Imperial College Press*. London, 2000.

[20] S. Vinson and L.D. Cohen. Multiple rectangle model for buildings segmentation and 3D scene reconstruction. In *Proc. International Conference on Pattern Recognition (ICPR)*, Quebec, Canada, 2002.

[21] U. Weidner and W. Forstner. Fowards Automatic Building Reconstruction from High Resolution Digital Elevation Models. *Journal of Photogrammetry and Remote Sensing*, 50(4):38–49, 1995.

Unité de recherche INRIA Sophia Antipolis
2004, route des Lucioles - BP 93 - 06902 Sophia Antipolis Cedex (France)

Unité de recherche INRIA Futurs : Parc Club Orsay Université - ZAC des Vignes
4, rue Jacques Monod - 91893 ORSAY Cedex (France)
Unité de recherche INRIA Lorraine : LORIA, Technopôle de Nancy-Brabois - Campus scientifique
615, rue du Jardin Botanique - BP 101 - 54602 Villers-lès-Nancy Cedex (France)
Unité de recherche INRIA Rennes : IRISA, Campus universitaire de Beaulieu - 35042 Rennes Cedex (France)
Unité de recherche INRIA Rhône-Alpes : 655, avenue de l'Europe - 38334 Montbonnot Saint-Ismier (France)
Unité de recherche INRIA Rocquencourt : Domaine de Voluceau - Rocquencourt - BP 105 - 78153 Le Chesnay Cedex (France)

Éditeur
INRIA - Domaine de Voluceau - Rocquencourt, BP 105 - 78153 Le Chesnay Cedex (France)
http://www.inria.fr
ISSN 0249-6399